

Cell-Free Bistatic Backscatter Communication: Channel Estimation, Optimization, and Performance Analysis

Diluka Galappaththige*, *Member, IEEE*, Fatemeh Rezaei*, *Member, IEEE*, Chintha Tellambura, *Fellow, IEEE*, Amine Maaref, *Senior Member, IEEE*

Abstract—This study introduces and investigates the integration of a cell-free architecture with bistatic backscatter communication (BiBC), referred to as cell-free BiBC or distributed access point (AP)-assisted BiBC, which can enable potential applications in future (EH)-based Internet-of-Things (IoT) networks. To that purpose, we first present a pilot-based channel estimation scheme for estimating the direct, cascaded, forward channels of the proposed system setup. We next utilize the channel estimates for designing the optimal beamforming weights at the APs, reflection coefficients at the tags, and reception filters at the reader to maximize the tag sum rate while meeting the tags' minimum energy requirements. Because the proposed maximization problem is non-convex, we propose a solution based on alternative optimization, fractional programming, and Rayleigh quotient techniques. We also quantify the computational complexity of the developed algorithms. Finally, we present extensive numerical results to validate the proposed channel estimation scheme and optimization framework, as well as the performance of the integration of these two technologies. Compared to the random beamforming/combining benchmark, our algorithm yields impressive gains. For example, it achieves $\sim 64.8\%$ and $\sim 253.5\%$ gains in harvested power and tag sum rate, respectively, for 10 dBm with 36 APs and 3 tags.

Index Terms—Backscatter communication systems, Semi-passive tags, Channel estimation, Resource allocation.

I. INTRODUCTION

With the rapid deployment of fifth-generation (5G) and beyond 5G (B5G) communication networks, energy harvesting (EH)-based Internet-of-Things (IoT) is becoming an extremely active research area, and the third-generation partnership project (3GPP) has launched a new study item [1]–[3]. These research items identify the following essential aspects and aims of EH-based IoT networks:

- Use cases such as identification, tracking, monitoring, actuating, and sensing for applications in logistics, transportation, healthcare, and others.
- Exploring public/private networks, indoor/outdoor environments, macro/micro/pico cells, cell-free connectivity to user equipment (UEs) with or without relay/UE assistance, and frequency bands (both licensed and unlicensed).
- Establishing EH techniques, connectivity requirements, and positioning accuracy.

*D. Galappaththige and F. Rezaei contributed equally to this work.

D. Galappaththige, F. Rezaei, and C. Tellambura with the Department of Electrical and Computer Engineering, University of Alberta, Edmonton, AB, T6G 1H9, Canada (e-mail: {diluka.lg, rezaei, ct4}@ualberta.ca).

A. Maaref is with Huawei Canada, 303 Terry Fox Drive, Suite 400, Ottawa, Ontario K2K 3J1 (e-mail: amine.maaref@huawei.com).

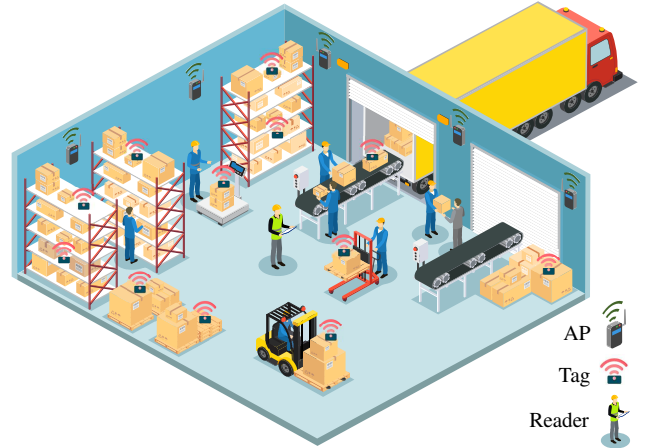


Fig. 1: A warehouse use case of cell-free BiBC network.

These challenges open a vast array of research questions. Very few of those have been explored [4], [5]. Inspired by them, we consider the problem of supporting the energy needs of multiple tags over a large coverage area such as a warehouse with a bistatic backscatter (BiBC) network of dedicated access points (APs)/radio frequency (RF) sources (see Fig. 1). Furthermore, these inexpensive backscatter tag-assisted IoT networks have numerous applications, including logistics, inventory management, warehousing, manufacturing, energy industry, healthcare, agriculture, aerospace and defense, farming, retail, sports, and many more. The potential market will grow at an exponential rate; for example, parcel volume in China will reach 163.4 billion by 2025 and 220-262 billion globally by 2026 [1]–[3]. These possible use cases offer significant market opportunities.

In scenarios like those mentioned, backscatter tags are favored due to their cost-effectiveness and minimal energy consumption (a few nW- μ W). They reflect RF signals from the RF source to transmit data to a reader, whether it is a dedicated or cooperative one [4]–[6], thus optimizing spectrum utilization and reducing the need for additional spectrum allocations. Tags find utility in IoT networks, enhancing both spectrum and energy efficiency [4]–[6]. Among the three backscatter network types (monostatic, bistatic, and ambient) [4], [5], BiBC systems excel in applications like warehouses. These systems employ dedicated RF sources, single or multiple, to power tags and enable backscatter modulation [4], [5]. In the context of BiBC, dedicated RF sources offer advantages over ambient

signals, including predictability, reduced interference, system control, and knowledge of source signal parameters. These advantages can be harnessed to optimize system coverage and performance [4], [5].

A. Technical Challenges in BiBC

Despite their wide application potential, several critical challenges constrain the performance of BiBC systems.

- 1) First, the dedicated RF sources (power beacons) in BiBC are primarily designed to provide energy wirelessly to tags. Power beacons offer localized coverage, providing energy within a specific area. Tags have EH circuits to convert the dedicated RF signals to direct current [4]. Specifically, the performance of the EH circuits depends on the activation threshold, typically around -20 dBm [7] or more of incident RF power. Hence, depending on the proximity to the power beacon, tags may not receive adequate power to activate EH and perform data backscattering. This causes energy outages at the tags and short activation ranges (a few meters). Hence, a single power beacon supporting multiple tags limits the tag performance while increasing the probability of an energy outage. Consequently, supporting a large number of tags across a broader area may need multiple power beacons.
- 2) Second, as tags backscatter their data, tag signals experience double path losses and deeper fading, leading to short communication distances (≤ 6 m), low data rates (≤ 1 bps/Hz), and low reliability [4], [5]. While connecting multiple tags is vital in applications, mutual interference caused by concurrent tag transmissions degrades the network performance. Hence, sophisticated signal processing techniques, e.g., beamforming design, interference cancellation schemes, and multiple access schemes are essential to increase reliability while establishing massive connectivity.
- 3) Third, optimal beamforming design, effective suppression of the direct link interference from the power beacon, and accurate data decoding of tags critically depend on the availability of perfect channel state information (CSI). However, the inherent limitations in the power and processing capabilities of tags, which simply backscatter incident RF signals, introduce substantial challenges to the channel estimation process. This complexity is further compounded in scenarios involving multiple power beacons and multiple tags. Thus, sophisticated methods are required for precise estimation of the direct channel ($\mathbf{h}_{0,m}$), forward channel ($f_{k,m}$), and the cascaded channels ($f_{mk}\mathbf{g}_k$) – Fig. 2.

B. Motivation and Our Contributions

Inspired by the aforementioned challenges in BiBC, as well as significant gaps in the literature to address the needs of EH-based IoT networks, we propose supporting multiple tags over a large coverage area such as a warehouse with a BiBC network of dedicated distributed APs, i.e., a cell-free BiBC system.

The basic concept behind cell-free networks is that a large number of spatially distributed APs serve multiple users on the same time-frequency resources. It thus minimizes transmission distances while increasing coverage, resulting in increased macro-diversity and favorable propagation [8]–[10]. Hence, by shortening AP-tag distances, the cell-free architecture can alleviate the limited energy availability and adverse effects of path loss in BiBC [11]–[14]. Furthermore, a central processing unit (CPU) coordinates the APs that are connected to it via a front-haul/back-haul link, allowing the APs to serve users in the area collaboratively. The distributed APs in the BiBC network can thus employ the jointly designed beamforming weights to deliver as much power to the tags as possible while minimizing inter-tag interference to support a large number of tags.

Integrating cell-free architecture with BiBC poses several critical technical challenges, such as (i) channel estimation (ii) enabling multi-tag transmission, (iii) AP beamforming strategies, (iv) tags' reflection coefficients/power allocation, (v) designing reader reception filters, (vi) minimum energy for tag activation, (vii) coverage, (viii) coexistence with conventional cellular networks, and more. Although none of these challenges have been thoroughly investigated, [11]–[14] address some of them (Section I-C). Hence, to address these challenges while filling a significant gap in the literature, we propose a generalized cell-free BiBC system (Fig. 2).

In particular, in the channel training phase, APs operate in full-duplex (FD) mode and use a TDMA scheme, i.e., an on-off switching protocol that is controlled by the CPU, to estimate the direct (APs-reader), cascaded (APs-tags-reader), and forward (APs-tags) channels using specially designed pilot sequences. During the data transmission, the APs operate in half-duplex (HD) mode and cooperate to service the tags in the area by beamforming to improve the tags' rate performance at the reader while ensuring the tags' minimum energy requirements for tag activation. We thus design the optimal AP beamforming weights, tags' reflection coefficients, and reader's combing filters to maximize the tags' sum rate, while meeting the EH requirements at the tags. We also take into account the effect of estimated CSI while designing the aforementioned AP beamforming weights, tag reflection coefficients, and reader combing filters.

The main contributions of this paper can be summarized as follows:

- 1) Using a specifically developed pilot sequence presented in [15], we propose a method to estimate the channels of the cell-free BiBC system, including direct, cascaded, and forward channels. During this phase, an on-off switching protocol is adopted and the APs operate in FD mode. We thus derive least squares (LS) and minimum mean square error (MMSE) estimators for these channels.
- 2) Following that, we formulate the tag sum rate maximization problem by optimizing the beamforming weights at the APs, reflection coefficients at the tags, and receiver combiner at the reader, while also maintaining the EH requirements at the tags. The formulated optimization

problem also accounts for the estimated CSI and CSI estimation errors.

- 3) The resulting maximizing problem has a non-convex objective function and constraints. Convex problems, on the other hand, can be solved efficiently with polynomial convergence time using readily available and widely accessible convex solvers. Therefore, we use the alternating optimization (AO) technique to decouple the non-convex problem into three sub-problems. Using this method, we develop solution algorithms for these sub-problems utilizing fractional programming (FP) and Rayleigh ratio quotient approaches.
- 4) We show that the proposed channel estimation scheme and optimization frameworks improve backscatter tag performance significantly in cell-free BiBC. We also investigate the algorithms' robustness to CSI errors and the computational complexities.
- 5) We also investigate the effects of fixed reflection coefficients at the tags. In particular, while these tags have lower performance than reconfigurable tags, i.e., tags with variable reflection coefficients, they could be a low-cost networking solution for particular applications.
- 6) Finally, we provide comprehensive numerical examples that demonstrate the performance of the proposed channel estimation scheme and cell-free BiBC network using the proposed solution.

Before proceeding to the technical contributions, we provide an overview of related works that attempt to address the BiBC problems outlined in Section I-A.

C. Previous Contribution on BiBC Systems

While no prior literature thoroughly addresses all the BiBC challenges, previous studies [12], [14], [16]–[18] tackled some of them. In particular, [12], [14] utilize a set of distributed RF sources to extend the coverage distance, thereby overcoming the tag's power limitations. Reference [12] specifically investigates the placement of power beacons to maximize the coverage distance taking into account the outage probability, while [14] explores tag-to-tag communication and investigates the performance of network coverage and capacity. These works, however, consider single antenna nodes and overlooked the importance of beamforming designs.

On the other hand, [16]–[18] focus on the performance studies of a BiBC with a single tag and a single RF source. In particular, [16] modifies the tag architecture to adjust the circuit load impedance of the tag to extend the communication range and lower the integrated circuit (IC) power consumption. The works [17], [18] develop interference cancellation schemes to suppress the direct link interference from the RF source, thereby improving the tag's rate. [17] uses beamforming to nullify the direct link interference, while [18] explores the joint design of waveform at the RF source and coding at the tag to mitigate the direct link interference. To further support multiple tags, [19] and [20] respectively adopt non-orthogonal multiple access (NOMA) and time division multiple access (TDMA) schemes. [19] maximizes the minimum tag rate by optimizing transmit beamforming at the source, receive

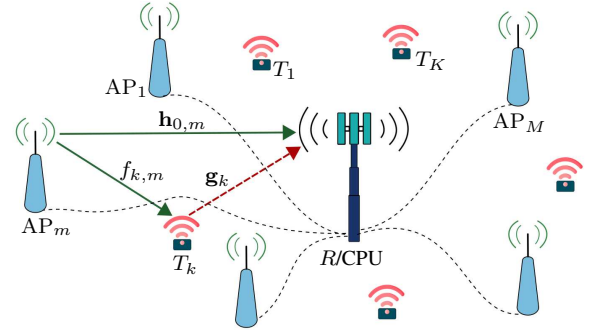


Fig. 2: Cell-free BiBC setup.

beamforming at the reader, and reflection coefficients at the tags. Whereas, [20] minimizes the transmit power level/energy consumption at the emitter by jointly optimizing the transmission time slot duration and tag reflection coefficients. Reference [21] also investigates the emitter power allocation and energy consumption considering a separate reader for each tag.

Leveraging the concept of distributed RF sources, the authors in [13] and [11] further explore beamforming design at distributed cellular APs serving a cellular user and a tag. They also consider channel estimation through pilot transmissions from the cellular APs. Channel estimation has been also investigated in BiBC using a pilot-based two-phase channel estimation protocol [17], [22]. However, no method exists for estimating the channels of a generalized BiBC network comprising multiple RF sources, multiple tags, and a reader.

The most relevant works are summarized in Table I, highlighting the unique contribution of this paper.

D. Structure and Notation

This paper is organized as follows: Section II first introduces the system model, channel model, and EH at the tags. Next, it discusses pilot transmission and channel estimation. Further, it presents the data transmission model and the achievable rates of the tags. In Section III, we formulate the sum rate maximization problem. We present the AO solution for the proposed problem in Section IV. In Section V, simulation examples are presented for performance evaluations. Section VI concludes the paper and outlines future research directions.

Notation: Lowercase bold and uppercase bold denote vectors and matrices. \mathbf{I}_n is the $n \times n$ identity matrix. \mathbf{A}^T and \mathbf{A}^H , denote transpose and Hermitian transpose, respectively. $\mathbb{E}\{\cdot\}$ denotes the statistical expectation. Finally, $\mathcal{CN}(\boldsymbol{\mu}, \mathbf{R})$ is a complex Gaussian vector with mean $\boldsymbol{\mu}$ and co-variance matrix \mathbf{R} . Finally, $\mathcal{M} = \{1, \dots, M\}$, $\mathcal{K} = \{1, \dots, K\}$, and $\mathcal{K}_k = \mathcal{K}/k$.

II. SYSTEM, CHANNEL, AND SIGNAL MODELS

A. System Model

We consider a cell-free BiBC system with M dedicated hybrid access point (H-AP), denoted by $AP_m, m \in \mathcal{M}$, K single-antenna tags, denoted by $T_k, k \in \mathcal{K}$, and a L -antenna reader, denoted by R (Fig. 2). Each H-AP equipped

TABLE I: Summary of related works.

Conf.	Ref.	Setup			Objective	EH Constraint	Variables [†]	Methodology	CSI Estimation
		APs	Tags	Reader					
AmBC	[11]	$M \geq 1$	$K = 1$	$L = 1$	Tag's rate	\times	\mathbf{w}	SCA	\checkmark
	[12]	$M \geq 1$	$K \geq 1$	$L = 1$	Coverage distance	\times	AP location	–	\times
BiBC	[19] [‡]	$M = 1$	$K \geq 1$	$L \geq 1$	Minimum Tag rate	\times	$\mathbf{w}, \mathbf{u}, \alpha$	AO & SCA	\times
	[20]	$M = 1$	$K \geq 1$	$L = 1$	Transmit power	\checkmark	p_t, α	SCA & BCD	\times
	[21]	$M = 1$	$K \geq 1$	$L = 1$	Energy efficiency	\checkmark	p_t, α	Lagrange dual decomposition	\times
	This paper	$M \geq 1$	$K \geq 1$	$L \geq 1$	Tags' sum rate	\checkmark	$\mathbf{w}, \mathbf{u}, \alpha$	AO & FP & Rayleigh ratio quotient	\checkmark

[†] The variables p_t , \mathbf{w} , \mathbf{u} , and α , denote transmit power, transmit beamforming, reception filter, and reflection coefficient.

SCA - successive convex approximation. BCD - block coordinated decent.

[‡] This work adopts NOMA to establish multiple access.

with a single antenna operates in either FD or HD mode [23]. Specifically, in FD mode, the antenna of an H-AP simultaneously excites a carrier signal and receives signals reflected by tags. We assume the perfect FD operation with perfect self-interference cancellation at the H-AP's decoupler [24], [25]. Each tag modulates its own data on the RF signals transmitted by the H-APs and transmits the modulated signals to the reader. We assume that the reader comprises a CPU, which is connected to all H-APs via a front-haul/back-haul link [26]. Hence, this front-haul/back-haul connection assists to share the necessary CSI between the reader and the H-APs. It also assists in the synchronization between all APs to simultaneously serve all tags in the same time-frequency resource block by adopting spatial multiplexing rendered by cell-free massive MIMO.

B. Channel Model

We consider a block flat-fading channel model. During each fading block, $\mathbf{h}_{0,m} \in \mathbb{C}^{L \times 1}$, $f_{k,m} \in \mathbb{C}$, and $\mathbf{g}_k \in \mathbb{C}^{L \times 1}$ denote the channels between AP_m – R, AP_m – T_k, and T_k – R, respectively. Moreover, $\mathbf{h}_{k,m} = f_{k,m} \mathbf{g}_k \in \mathbb{C}^{L \times 1}$ denotes the cascaded channel between AP_m – T_k – R. A unified representation of all individual channels is given as

$$\mathbf{v} = \zeta_v^{1/2} \tilde{\mathbf{v}}, \quad (1)$$

where $\mathbf{v} \in \{\mathbf{h}_{0,m}, f_{k,m}, \mathbf{g}_k\}$. In (1), ζ_v captures the large-scale path-loss and shadowing, which stays constant for several coherence intervals. Hence, the channel statistics at the H-APs and reader are assumed to be known a-prior since they change very slowly. Moreover, $\tilde{\mathbf{v}} \sim \mathcal{CN}(\mathbf{0}, \mathbf{I}_N)$ accounts for the small-scale Rayleigh fading¹, where $N \in \{L, 1\}$.

C. EH at Tags

In the considered system, tags are assumed to be semi-passive tags with small energy storage [27]. In particular, tags only use the stored energy during the channel estimation phase. Otherwise, tags perform EH and data transmission simultaneously via the power-splitting mode in the data transmission phase [27].

During data transmission, T_k reflects $\alpha_k P_k$ for data transmission and absorbs $P_k^{in} = (1 - \alpha_k) P_k$, for EH, where P_k is

¹Note that $f_{k,m} = \zeta_{f_{k,m}}^{1/2} \tilde{f}_{k,m}$ and $\tilde{f}_{k,m} \sim \mathcal{CN}(0, 1)$.

incident RF power and $\alpha_k \in (0, 1)$ is the reflection coefficient of T_k. The EH circuit converts P_k^{in} to direct current (DC) power to perform internal operations and refill the energy storage [4]. The amount of harvested power at T_k, $P_{h,k}$, can be modeled as a linear or nonlinear function of the incident RF power. The linear model is the most widely used in the literature due to its simplicity but ignores the non-linear characteristics of actual EH circuits such as saturation and sensitivity. For that reason, several non-linear models have been developed [28]. In particular, for the nonlinear model, $P_{h,k} = \Phi(P_k^{in})$, where $\Phi(\cdot)$ is the nonlinear EH function [29, Eqn. (2)], and for the linear model, $P_{h,k} = \eta_b P_k^{in}$, where $\eta_b \in (0, 1)$ is the power conversion efficiency, which is typical $\eta_b = \{0.2, 0.4, 0.6\}$ [27]. Fortunately, both linear and non-linear models can be handled under a single unified framework, as we show next.

In order to activate the tag, the harvested power should exceed the threshold, i.e., $P_{h,k} \geq p_b$. The threshold is about –20 dBm for commercial passive tags [4]. In particular, $P_k^{in} \geq p'_b$, where $p'_b \triangleq \Phi^{-1}(p_b)$ for nonlinear EH model and $p'_b = p_b/\eta_b$ for linear EH case.

D. Pilot Transmission and Channel Estimation

In our study, we adopt a cell-free BiBC system operating in the time division duplex (TDD) transmission mode for both channel estimation and data transmission [30]. TDD, a widely used multiple-access technique, allocates distinct time slots for uplink (UL) and downlink (DL) transmissions over a single channel. This characteristic makes TDD an efficient choice in terms of spectrum utilization [31], as it allows dynamic allocation of time slots without the need to modify the bandwidth. This flexibility is beneficial in meeting diverse application requirements and ensuring the quality of service [31], making TDD particularly suitable for scenarios with unpaired spectrum and asymmetric data rate needs. One of the advantages of TDD over frequency division duplex (FDD) is its simplified channel equalization methods, emanating from the principle of channel reciprocity [31]. This simplification reduces the complexity of the system while maintaining reliable communication performance. In sum, Our choice of TDD for the cell-free BiBC system is justified by its spectrum efficiency, dynamic resource allocation, and simplicity compared to FDD [31].

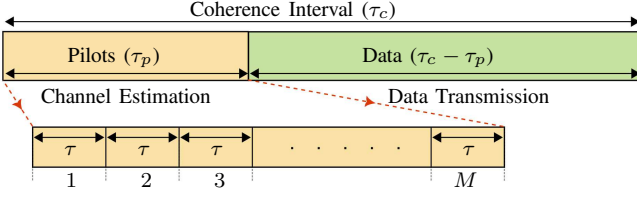


Fig. 3: Transmission framework.

Accurate estimation of the channels is necessary to fully benefit from cell-free BiBC. In particular, the CSI of forward channels, i.e., $f_{k,m}$ for $m \in \mathcal{M}, k \in \mathcal{K}$, and the cascaded channels, i.e., $\mathbf{h}_{k,m}$ for $m \in \mathcal{M}, k \in \mathcal{K}$, is crucial for designing beamforming at APs, reflection coefficients at tags, and reception filters at the reader while guaranteeing EH and rate performance. On the other hand, the reader requires accurate information about the direct channels, i.e., $\mathbf{h}_{0,m}$ for $m \in \mathcal{M}$, to suppress the direct link interference before decoding the tags' data. By accurately estimating these channels, the BiBC system's performance can be enhanced by improving signal quality and successfully decoding data transmitted by tags.

Following the methodology presented in [15], we employ a pilot-based channel estimation scheme to estimate $\mathbf{h}_{0,m}$, $\mathbf{h}_{k,m}$, and $f_{k,m}$ for $m \in \mathcal{M}$ and $k \in \mathcal{K}$. We assume that in each coherence block of length τ_c , $\tau_p (< \tau_c)$ samples are used for channel estimation (Fig. 3). During the channel estimation phase, we adopt a TDMA scheme, using an on-off switching protocol that is controlled by the CPU. Specifically, the channel estimation duration τ_p is divided into M slots, each with length $\tau \geq K + 1$, and $\tau_p = M\tau$. In each time slot, the CPU activates a specific AP in FD mode to transmit a pilot sequence $\mathbf{s} = [s_1, \dots, s_\tau] \in \mathbb{C}^{1 \times \tau}$, while the remaining APs are turned off. Here, s_i satisfies $|s_i|^2 = 1$ for $i = \{1, \dots, \tau\}$. In the given time slot, all the tags are active and backscatter the AP signal to transmit their pilot signals, i.e., T_k backscatters $\mathbf{c}_k = [c_{k1}, \dots, c_{k\tau}] \in \mathbb{C}^{1 \times \tau}$, where c_{ki} is the tag's transmit pilot symbol over the i th AP symbol, s_i . The reader estimates the direct and cascaded channels using the tags' backscattered signals and the activated AP signal, whereas the activated AP estimates the forward channels using the tags' backscattered signals.

Remark 1. For evaluating channel estimation performance, we assume that the tags use modified Zadoff-Chu (ZC) sequences as pilots, \mathbf{c}_k , as in [15]. However, other sequences, such as rows of Hadamard Matrix, can be used to estimate the channels. Furthermore, according to Theorem 4 in [15], any set of orthogonal sequences can be modified for backscatter channel estimation based on the characteristics of the tag's RF front end, the complexity of the tag itself, and the application environment.

The received signals at the reader at the m th time slot, over τ pilot symbols, can be expressed as [15]

$$\mathbf{Y}_m = \sqrt{p_p} \mathbf{H}_m \mathbf{X} \mathbf{S} + \mathbf{N}_m, \quad (2)$$

where p_p is the pilot transmit power, $\mathbf{H}_m = [\mathbf{h}_{0,m}, \sqrt{\alpha_1} \mathbf{h}_{1,m}, \dots, \sqrt{\alpha_K} \mathbf{h}_{K,m}] \in \mathbb{C}^{L \times (K+1)}$, $\mathbf{S} \triangleq \text{diag}(\mathbf{s})$, and $\mathbf{N}_m \in \mathbb{C}^{L \times \tau}$ is the noise

matrix with i.i.d $\mathcal{CN}(0, \sigma^2)$ elements. In (2), $\mathbf{X} = [\mathbf{x}_1, \dots, \mathbf{x}_\tau] \in \mathbb{C}^{(K+1) \times \tau}$, includes the transmitted pilots by the tags, $\mathbf{x}_i = [1, c_{1i}, \dots, c_{Ki}]^T \in \mathbb{C}^{(K+1) \times 1}$, and $\mathbf{X} \mathbf{X}^H = \tau \mathbf{I}_{K+1}$.

In order to estimate \mathbf{H}_m , by projecting the received signal (2) onto \mathbf{S}^H , the post-processed received signal is given as

$$\bar{\mathbf{Y}}_m = \sqrt{p_p} \mathbf{H}_m \mathbf{X} + \bar{\mathbf{N}}_m, \quad (3)$$

where $\bar{\mathbf{N}}_m = \mathbf{N}_m \mathbf{S}^H \in \mathbb{C}^{L \times \tau}$ is the noise matrix with i.i.d $\mathcal{CN}(0, \sigma^2)$ elements.

The reader then correlates the received pilot signal in (3) with \mathbf{X} , which results in a de-spreading operation. The post-processed signal is thus given as

$$\bar{\mathbf{Y}}_{m,p} = \bar{\mathbf{Y}}_m \mathbf{X}^H / \tau = \sqrt{p_p} \mathbf{H}_m + \bar{\mathbf{N}}_{m,p}, \quad (4)$$

where $\bar{\mathbf{N}}_{m,p} = \bar{\mathbf{N}}_m \mathbf{X}^H / \tau$ having i.i.d $\mathcal{CN}(0, \sigma_p^2)$ elements, where $\sigma_p^2 = \sigma^2 / \tau$. Given independent Rayleigh fading, the elements of the channel matrix and the noise matrix are statistically independent. Next, the (l, k) th element of (4) is given as

$$[\bar{\mathbf{Y}}_{m,p}]_{l,k} \triangleq y_{l,k}^m = \sqrt{p_p} h_{l,k}^m + n_{l,k}^m, \quad (5)$$

where $h_{l,k}^m = [\mathbf{H}_m]_{l,k}$ and $n_{l,k}^m = [\bar{\mathbf{N}}_{m,p}]_{l,k}$.

The MMSE estimator is thus given as [15]

$$\begin{aligned} \hat{h}_{l,k}^m &= \mathbb{E}\{h_{l,k}^m | y_{l,k}^m\} = \frac{\mathbb{E}\{\bar{h}_{l,k}^m (y_{l,k}^m)^*\}}{\mathbb{E}\{|y_{l,k}^m|^2\}} y_{l,k}^m \\ &= \begin{cases} \frac{\sqrt{p_p} \zeta_{\mathbf{h}_{0,m}}}{p_p \zeta_{\mathbf{h}_{0,m}} + \sigma_p^2} y_{l,0}^m, & \text{for } k = 0, \\ \frac{\sqrt{\alpha_k p_p} \zeta_{\mathbf{h}_{k,m}}}{\alpha_k p_p \zeta_{\mathbf{h}_{k,m}} + \sigma_p^2} y_{l,k}^m, & \text{for } k \in \mathcal{K}, \end{cases} \end{aligned} \quad (6)$$

where $\zeta_{\mathbf{h}_{k,m}} = \zeta_{f_{k,m}} \zeta_{\mathbf{g}_k}$.

Thus, the MMSE estimate of the complete channel matrix, \mathbf{H}_m , is given as

$$\hat{\mathbf{H}}_m^{\text{MMSE}} = \mathbf{Y}_{m,p} \mathbf{D}_{m,\gamma}^{1/2}, \quad (7)$$

where $\mathbf{D}_{m,\gamma} = \text{diag}([\gamma_{0,m}, \gamma_{1,m}, \dots, \gamma_{K,m}])$, in which $\gamma_{0,m} = \frac{p_p \zeta_{\mathbf{h}_{0,m}}^2}{p_p \zeta_{\mathbf{h}_{0,m}} + \sigma_p^2}$ and $\gamma_{k,m} = \frac{\alpha_k p_p \zeta_{\mathbf{h}_{k,m}}^2}{\alpha_k p_p \zeta_{\mathbf{h}_{k,m}} + \sigma_p^2}$.

Additionally, using (2), the LS estimate which operates without any prior knowledge of the channel can be obtained as

$$\hat{\mathbf{H}}_m^{\text{LS}} = \mathbf{Y}_m \bar{\mathbf{X}}^\dagger, \quad (8)$$

where $\bar{\mathbf{X}}^\dagger = \mathbf{X}^H (\bar{\mathbf{X}} \bar{\mathbf{X}}^H)^{-1}$, where $\bar{\mathbf{X}} = \sqrt{p_p} \mathbf{X}$.

Similarly, the received signal at AP $_m$ over τ pilot symbols can be expressed as

$$\mathbf{y}_m^p = \sqrt{p_p} \sum_{i \in \mathcal{K}} \sqrt{\alpha_i} f_{i,m}^T f_{i,m} \mathbf{c}_i \mathbf{S} + \mathbf{n}_m. \quad (9)$$

where $\mathbf{n}_m \in \mathbb{C}^{1 \times \tau} \sim \mathcal{CN}(\mathbf{0}, \sigma_a^2 \mathbf{I}_\tau)$ denotes the noise at AP $_m$. The post-processed received signal is thus given as

$$\bar{\mathbf{y}}_m^p = \mathbf{y}_m^p \mathbf{S}^H = \sqrt{p_p} \sum_{i \in \mathcal{K}} \sqrt{\alpha_i} f_{i,m}^T f_{i,m} \mathbf{c}_i + \bar{\mathbf{n}}_m, \quad (10)$$

where $\bar{\mathbf{n}}_m = \mathbf{n}_m \mathbf{S}^H$. The received pilot signal is then projected onto the \mathbf{c}_k^H which yields

$$y_{k,m}^p = \bar{\mathbf{y}}_m^p \mathbf{c}_k^H / \tau = \sqrt{p_p \alpha_k} f_{k,m}^T f_{k,m} + n_{k,m}, \quad (11)$$

where $n_{k,m} = \bar{\mathbf{n}}_m \mathbf{c}_i^H / \tau \sim \mathcal{CN}(0, \sigma_a^2 / \tau)$.

Therefore, the LS estimate of $f_{k,m} = f_{k,m}^T f_{k,m}$ can be obtained as²

$$\hat{f}_{k,m}^{\text{LS}} = y_{k,m}^p / \sqrt{p_p \alpha_k}. \quad (12)$$

Hence, we can obtain an approximate estimate for the forward channel, $f_{k,m}$, using the estimates of $\bar{f}_{k,m}$, as $\hat{f}_{k,m}^{\text{LS}} \approx \sqrt{\hat{f}_{k,m}^{\text{LS}}}$.

E. Transmission Model

All APs simultaneously serve the tags in HD mode in the data transmission phase. The signal transmitted at AP_m is thus given as

$$q_m = \sqrt{p_t} \sum_{i \in \mathcal{K}} w_{i,m} s, \quad (13)$$

where p_t is the transmit power at each AP, $w_{i,m} \in \mathbb{C}$ is the spatial directivity/precoder of the signal at AP_m for T_i , and $s \sim \mathcal{CN}(0, 1)$ is the carrier signal satisfying $\mathbb{E}\{|s|^2\} = 1$. The signal received at T_k is given as

$$y_k = \mathbf{f}_k^T \mathbf{q} = \sqrt{p_t} \sum_{i \in \mathcal{K}} \mathbf{f}_k^T \mathbf{w}_i s, \quad (14)$$

where $\mathbf{q} = [q_1, \dots, q_M]^T \in \mathbb{C}^{M \times 1}$, and $\mathbf{w}_i = [w_{1i}, \dots, w_{Mi}]^T \in \mathbb{C}^{M \times 1}$. Moreover, $\mathbf{f}_k = [f_{k,1}, \dots, f_{k,M}]^T \in \mathbb{C}^{M \times 1}$ denotes the effective channel between all APs and T_k .

The tags must harvest enough power to support their internal operations. Hence, the input signal power at EH circuit of T_k must satisfy the following energy constraint (Section II-C):

$$P_k^{\text{in}} = (1 - \alpha_k) p_t \left| \sum_{i \in \mathcal{K}} \mathbf{f}_k^T \mathbf{w}_i \right|^2 \geq p'_b, \quad (15)$$

where $p'_b \triangleq \Phi^{-1}(p_b)$ for nonlinear EH model and $p'_b = p_b / \eta_b$ for linear EH case. T_k harvests energy from the received signal and modulates it with its data, c_k , where c_k is the normalized backscatter symbol selected from a multi-level (M -ary) modulation such that $\mathbb{E}\{|c_k|^2\} = 1$, before sending it to the reader. The received signal at the reader is thus given as

$$\begin{aligned} \mathbf{r} &= \sum_{m \in \mathcal{M}} \mathbf{h}_{0,m} q_m + \sum_{j \in \mathcal{K}} \sqrt{\alpha_j} \mathbf{g}_j y_j c_j + \mathbf{z} \\ &= \mathbf{H}_0 \mathbf{q} + \sqrt{p_t} \sum_{j \in \mathcal{K}} \sum_{i \in \mathcal{K}} \sqrt{\alpha_j} \mathbf{g}_j \mathbf{f}_i^T \mathbf{w}_i s c_j + \mathbf{z}, \end{aligned} \quad (16)$$

where $\mathbf{H}_0 = [\mathbf{h}_{0,1}, \dots, \mathbf{h}_{0,M}] \in \mathbb{C}^{L \times M}$, and $\mathbf{z} \in \mathbb{C}^{L \times 1} \sim \mathcal{CN}(0, \sigma^2 \mathbf{I}_L)$ is the additive white Gaussian noise (AWGN) vector at the reader. In (16), the first term is the direct-link signals from the APs and the second term is the backscatter-link signals from tags.

Remark 2. The reader uses SIC to remove the direct-link signals from all APs and then applies the combining filter, $\mathbf{u}_k \in \mathbb{C}^{L \times 1}$ to decode T_k 's signal. Because direct channels between APs and the reader are conventional cell-free one-way channels, they can be estimated more accurately, i.e. with a lower normalized mean square error than backscatter

channels. Our simulation results also support the validity of this argument (Fig 4).

Following Remark 2, we assume that the reader is able to perfectly remove the direct APs' signals from the received signal (16). The post-processed signal for decoding T_k 's data at the reader is thus given as

$$\begin{aligned} r_k &= \mathbf{u}_k^T (\mathbf{r} - \mathbf{H}_0 \mathbf{q}) \\ &= \underbrace{\sqrt{\alpha_k p_t} \sum_{i \in \mathcal{K}} \mathbf{u}_k^T \mathbf{g}_i \mathbf{f}_i^T \mathbf{w}_i s c_i}_{\text{Desired signal}} \\ &\quad + \underbrace{\sqrt{p_t} \sum_{j \in \mathcal{K}_k} \sum_{i \in \mathcal{K}} \sqrt{\alpha_j} \mathbf{u}_k^T \mathbf{g}_j \mathbf{f}_i^T \mathbf{w}_i s c_j}_{\text{Interference from the tag}} + \underbrace{\mathbf{u}_k^T \mathbf{z}}_{\text{Noise}}, \end{aligned} \quad (17)$$

where the first, second, and third terms in r_k are respectively the desired signal, interference from other tags, and effective noise at the reader.

F. Achievable Rate

This section derives the achievable rates of the tags. Using (17), the received SINR for T_k , γ'_k , at the reader is obtained as

$$\gamma'_k = \frac{\alpha_k p_t \left| \sum_{i \in \mathcal{K}} \mathbf{u}_k^T \mathbf{g}_i \mathbf{f}_i^T \mathbf{w}_i \right|^2 |s|^2}{p_t \sum_{j \in \mathcal{K}_k} \alpha_j \left| \sum_{i \in \mathcal{K}} \mathbf{u}_k^T \mathbf{g}_j \mathbf{f}_i^T \mathbf{w}_i \right|^2 |s|^2 + \|\mathbf{u}_k\|^2 \sigma^2}. \quad (18)$$

Thus, the achievable rate of T_k at the reader is given as

$$\mathcal{R}_k = \psi \mathbb{E}_s \{\log_2(1 + \gamma'_k)\}, \quad (19)$$

where the pre-log factor $\psi = (\tau_c - \tau_p) / \tau_c$ captures the effective portion of the coherence interval for the DL transmission. By taking the average over s in (19), the rate of T_k is computed as³

$$\mathcal{R}_k = \psi \log_2(e) \left(-e^{-\frac{1}{a_k + b_k}} \text{E}_i \left(\frac{-1}{a_k + b_k} \right) + e^{-\frac{1}{b_k}} \text{E}_i \left(\frac{-1}{b_k} \right) \right), \quad (20)$$

where

$$a_k \triangleq \frac{\alpha_k p_t}{\|\mathbf{u}_k\|^2 \sigma^2} \left| \sum_{i \in \mathcal{K}} \mathbf{u}_k^T \mathbf{g}_i \mathbf{f}_i^T \mathbf{w}_i \right|^2, \quad (21a)$$

$$b_k \triangleq \frac{p_t}{\|\mathbf{u}_k\|^2 \sigma^2} \sum_{j \in \mathcal{K}_k} \alpha_j \left| \sum_{i \in \mathcal{K}} \mathbf{u}_k^T \mathbf{g}_j \mathbf{f}_i^T \mathbf{w}_i \right|^2. \quad (21b)$$

Additionally, $\text{E}_i(x) = \int_{-\infty}^x u^{-1} e^u du$ is the exponential integral function. Note that, $-e^{-\frac{1}{x}} \text{E}_i(-1/x)$ is monotonically increasing and concave function of x [30].

III. OPTIMIZATION PROBLEM FORMULATION

Herein, we optimize the performance of the proposed cell-free BiBC setup (Fig. 2). We aim to maximize the sum rate of the tags while ensuring the tag activation, i.e., the tags meet the minimum operational energy requirements. The optimization variables are APs' precoders, i.e., \mathbf{w}_k for $k \in \mathcal{K}$, the combining filters at the reader, i.e. \mathbf{u}_k for $k \in \mathcal{K}$, and the tags' reflection coefficients, i.e. α_k for $k \in \mathcal{K}$.

²For the forward link we only derive the LS estimator for brevity.

³For $s \sim \mathcal{CN}(0, 1)$, $|s|^2$ is exponentially distributed.

The sum rate maximization problem can be formulated as

$$\mathbf{P1} : \underset{\mathbf{w}_k, \mathbf{u}_k, \alpha_k, \forall k}{\text{maximize}} \sum_{k \in \mathcal{K}} \mathcal{R}_k, \quad (22a)$$

$$\text{subject to} \sum_{i \in \mathcal{K}} |w_{i,m}|^2 \leq 1, \quad (22b)$$

$$(1 - \alpha_k)p_t \left| \sum_{i \in \mathcal{K}} \mathbf{f}_k^T \mathbf{w}_i \right|^2 \geq p'_b, \quad (22c)$$

$$\|\mathbf{u}_k\|^2 \leq 1, \quad (22d)$$

$$0 < \alpha_k < 1. \quad (22e)$$

Here, (22b) is the per-AP transmit power constraint, (22c) is the minimum per-tag power requirement for EH, and (22d) is the normalization constraint for the combining filter at the reader.

Remark 3. In order to solve the proposed sum rate maximization problem, we replace the rate of each tag, given in (19), with the following bound for traceability [32]:

$$\mathcal{R}_k \approx \psi \log_2(1 + \mathbb{E}_s\{\gamma'_k\}) = \psi \log_2(1 + \gamma_k), \quad (23)$$

where

$$\gamma_k = \frac{\alpha_k p_t \left| \sum_{i \in \mathcal{K}} \mathbf{u}_k^T \mathbf{g}_k \mathbf{f}_k^T \mathbf{w}_i \right|^2}{p_t \sum_{j \in \mathcal{K}_k} \alpha_j \left| \sum_{i \in \mathcal{K}} \mathbf{u}_k^T \mathbf{g}_j \mathbf{f}_j^T \mathbf{w}_i \right|^2 + \|\mathbf{u}_k\|^2 \sigma_w^2}. \quad (24)$$

In addition, since the CPU/reader performs the optimization by using the estimated CSI of the channels, all of the objective functions and constraints in $\mathbf{P1}$ are substituted with their respective channel estimations.

The proposed sum rate maximization, $\mathbf{P1}$, has an objective function and constraints that are not convex functions in \mathbf{w}_k , \mathbf{u}_k , and α_k . Non-convex problems are hard to solve optimally. Such a problem may have multiple feasible regions and multiple locally optimal points within each region. The problem of finding the exact global solution of a non-convex problem is NP-hard. Therefore, we resort to decoupling the optimization variables and employ AO, FP, and Rayleigh ratio quotient approaches.

IV. PROPOSED SOLUTION

As mentioned before, the AO paradigm requires the optimization variables to be split into non-overlapping blocks of one or more block variables. This allows iterative optimization of one block variable at a time while holding the others fixed, then proceeds on to optimizing the next block while holding the others fixed, and so on until convergence is attained. This method is also known as block coordinate descent [33]. In our problem, \mathbf{w}_k , \mathbf{u}_k , and α_k are the natural choice of blocks.

A. Transmit Beamforming

When the tags' reflection coefficients and the reader's receiver combining are fixed, $\mathbf{P1}$ reduces to the following transmit beamforming optimization problem:

$$\mathbf{P}_w : \underset{\mathbf{w}_k \forall k}{\text{maximize}} \sum_{k \in \mathcal{K}} \psi \log_2(1 + \hat{\gamma}_k), \quad (25a)$$

$$\text{subject to} \sum_{i \in \mathcal{K}} |w_{i,m}|^2 \leq 1, \quad (25b)$$

$$(1 - \alpha_k)p_t \left| \sum_{i \in \mathcal{K}} \hat{\mathbf{f}}_k^T \mathbf{w}_i \right|^2 \geq p'_b, \quad (25c)$$

where $\hat{\gamma}_k$ is obtained by replacing the respective channels, i.e., \mathbf{g}_k and \mathbf{f}_k for $k \in \mathcal{K}$, in (24) with respective estimated channels.

Next, we define $\mathbf{a}_{kj} \triangleq [\mathbf{u}_k^T \hat{\mathbf{g}}_j \hat{\mathbf{f}}_j^T, \dots, \mathbf{u}_k^T \hat{\mathbf{g}}_j \hat{\mathbf{f}}_j^T] \in \mathbb{C}^{MK \times 1}$ and $\mathbf{w} \triangleq [\mathbf{w}_1^T, \dots, \mathbf{w}_K^T]^T \in \mathbb{C}^{MK \times 1}$. Thereby, the T_k 's SINR in (24) is rearranged as

$$\hat{\gamma}_k = \frac{\alpha_k p_t \left| \mathbf{a}_{kk}^T \mathbf{w} \right|^2}{p_t \sum_{j \in \mathcal{K}_k} \alpha_j \left| \mathbf{a}_{kj}^T \mathbf{w} \right|^2 + \sigma_w^2}, \quad (26)$$

where $\sigma_w^2 = \|\mathbf{u}_k\|^2 \sigma^2$. Then, \mathbf{P}_w can be treated as a multiple ratio FP problem [34], [35]. We next apply a quadratic transform to the objective function of \mathbf{P}_w as

$$f(\mathbf{w}, \boldsymbol{\lambda}) = \sum_{k \in \mathcal{K}} \psi \log_2 \left(1 + 2\lambda_k \sqrt{\alpha_k p_t} \text{Re} \{ \mathbf{a}_{kk}^T \mathbf{w} \} - \lambda_k^2 \left(p_t \sum_{j \in \mathcal{K}_k} \alpha_j \left| \mathbf{a}_{kj}^T \mathbf{w} \right|^2 + \sigma_w^2 \right) \right), \quad (27)$$

where $\boldsymbol{\lambda} = [\lambda_1, \dots, \lambda_K]^T$ is the auxiliary variable introduced by the quadratic transformation. Thereby, we alternatively optimize \mathbf{w} and $\boldsymbol{\lambda}$. For a given \mathbf{w} , the optimal $\boldsymbol{\lambda}$ is found in closed-form as [34]

$$\lambda_k^o = \frac{\sqrt{\alpha_k p_t} \text{Re} \{ \mathbf{a}_{kk}^T \mathbf{w} \}}{\ln(2) \left(p_t \sum_{j \in \mathcal{K}_k} \alpha_j \left| \mathbf{a}_{kj}^T \mathbf{w} \right|^2 + \sigma_w^2 \right)}. \quad (28)$$

Remark 4. Without losing generality, we constrain the transmit beamforming vector, \mathbf{w} , with the channel responses to obtain a non-negative real desired signal term, i.e., $|\mathbf{a}_{kk}^T \mathbf{w}| \approx \text{Re} \{ \mathbf{a}_{kk}^T \mathbf{w} \}$. Our simulation findings support the validity of this technique. This is due to the fact that our method iteratively maximizes the achievable rate/SINR by co-phasing the desired signal component while reducing interference.

Next, we must optimize \mathbf{w} for a given $\boldsymbol{\lambda}$. First, by applying several mathematical manipulations, the objective function in (27) can be rearranged as

$$f(\mathbf{w}) = \sum_{k \in \mathcal{K}} \psi \log_2 \left(1 - \mathbf{w}^T \mathbf{U}_k \mathbf{w} + 2 \text{Re} \{ \mathbf{w}^T \mathbf{v}_k \} + t_k \right), \quad (29)$$

where \mathbf{U}_k , \mathbf{v}_k , and t_k for $k \in \mathcal{K}$ are defined as

$$\mathbf{U}_k \triangleq (\lambda_k^o)^2 p_t \sum_{j \in \mathcal{K}_k} \alpha_j \mathbf{a}_{kj} \mathbf{a}_{kj}^T, \quad (30a)$$

$$\mathbf{v}_k \triangleq 2\lambda_k^o \sqrt{\alpha_k p_t} \mathbf{a}_{kk}, \quad (30b)$$

$$t_k \triangleq (\lambda_k^o)^2 \sigma_w^2. \quad (30c)$$

Next, for a given $\boldsymbol{\lambda}$, the corresponding optimization problem is given as

$$\mathbf{P}_{w1} : \underset{\mathbf{w}}{\text{maximize}} f(\mathbf{w}), \quad (31a)$$

$$\text{subject to} \sum_{i \in \mathcal{K}} |w_{i,m}|^2 \leq 1, \quad (31b)$$

$$(1 - \alpha_k)p_t P_k^{\text{Lin}} \geq p'_b, \quad (31c)$$

where P_k^{Lin} is the linearized received signal power at T_k , given as

$$P_k^{\text{Lin}} = \left(\mathbf{w}^{(i-1)} \right)^T \mathbf{D}_k \mathbf{w}^{(i-1)} + \left((\mathbf{D}_k + \mathbf{D}_k^T) \mathbf{w}^{(i-1)} \right)^T \left(\mathbf{w}^{(i)} - \mathbf{w}^{(i-1)} \right), \quad (32)$$

where $\mathbf{D}_k = \mathbf{d}_k \mathbf{d}_k^T$ and $\mathbf{d}_k \triangleq [\hat{\mathbf{f}}_k^T, \dots, \hat{\mathbf{f}}_k^T]^T \in \mathbb{C}^{MK \times 1}$. Besides, $\mathbf{w}^{(i)}$ and $\mathbf{w}^{(i-1)}$ are the current and the previous iteration values of \mathbf{w} .

Because $\mathbf{a}_{kj} \mathbf{a}_{kj}^T$ is a positive-definite matrix, \mathbf{U}_k is also a positive-definite matrix. Hence, the objective function, $f(\mathbf{w})$, is a quadratic concave function of \mathbf{w} . Consequently, \mathbf{P}_{w1} can be solved as a quadratically constrained quadratic program (QCQP) [36]. Algorithm 1 gives the solution of \mathbf{P}_{w1} .

Algorithm 1 : Transmit beamforming.

Initialization: Initialize \mathbf{w} to a feasible value.

Repeat

Step 1: Update λ by (28).

Step 2: Update \mathbf{w} by solving \mathbf{P}_{w1} in (31).

Until the value of the objective function converges.

Output: The optimal transmit beamforming vector \mathbf{w}^o .

Remark 5. The proposed optimization strategy for solving \mathbf{w} once the original problem, \mathbf{P}_w , is transformed into a convex problem is shown in Algorithm 1. An alternating optimization strategy is used to solve \mathbf{P}_w iteratively. We begin by quantifying the SINR in (24) upon initializing \mathbf{w} , and then we update a better solution for \mathbf{w} in each iteration. This process is repeated until the normalized objective function increases less than $\epsilon = 10^{-4}$.

B. Receiver Combining

Here, we design the reader's combining filters. To this end, for fixed transmit beamforming and tags' reflection coefficients, $\mathbf{P1}$ is reduced to a receiver combining optimization problem and is formulated as

$$\mathbf{P}_u : \underset{\mathbf{u}_k, \forall k}{\text{maximize}} \sum_{k \in \mathcal{K}} \psi \log_2(1 + \hat{\gamma}_k), \quad (33a)$$

$$\text{subject to } \|\mathbf{u}_k\|^2 \leq 1. \quad (33b)$$

We first define $\mathbf{b}_k \triangleq \mathbf{g}_k \sum_{i \in \mathcal{K}} \mathbf{f}_k^T \mathbf{w}_i$ and rewrite the T_k 's SINR in (24) as

$$\begin{aligned} \hat{\gamma}_k &= \frac{\alpha_k p_t |\mathbf{b}_k^T \mathbf{u}_k|^2}{p_t \sum_{j \in \mathcal{K}_k} \alpha_j |\mathbf{b}_j^T \mathbf{u}_k|^2 + \|\mathbf{u}_k\|^2 \sigma^2} \\ &= \frac{\mathbf{u}_k^T \mathbf{B}_k \mathbf{u}_k}{\mathbf{u}_k^T \left(\sum_{j \in \mathcal{K}_k} \mathbf{B}_j + \sigma^2 \mathbf{I}_L \right) \mathbf{u}_k}, \end{aligned} \quad (34)$$

where $\mathbf{B}_j = \alpha_j p_t \mathbf{b}_j \mathbf{b}_j^T$. Since the objective function in (33a) is a non-decreasing function of its argument, it can be replaced by the SINR of T_k (34), i.e., $\sum_{k \in \mathcal{K}} \log_2(1 + \hat{\gamma}_k) = \sum_{k \in \mathcal{K}} \hat{\gamma}_k$. \mathbf{P}_u thus becomes a generalized Rayleigh ratio quotient problem [37], [38]. Hence, the optimal combiner vector for T_k is given as [37], [38]

$$\mathbf{u}_k^o = v_{\max} \left[\left(\sum_{j \in \mathcal{K}_k} \mathbf{B}_j + \sigma^2 \mathbf{I}_L \right)^{-1} \mathbf{B}_k \right], \quad (35)$$

where $v_{\max}[\cdot]$ is the dominant eigenvector of the matrix [37], [38].

C. Reflection Coefficient Optimization

As the final block of the proposed AO framework, here, we optimize the tags' reflection coefficients. For given transmit beamforming and receiver combining, $\mathbf{P1}$ becomes an optimization problem for tags' reflection coefficients. The corresponding optimization problem is given as

$$\mathbf{P}_\alpha : \underset{\alpha_k, \forall k}{\text{maximize}} \sum_{k \in \mathcal{K}} \psi \log_2(1 + \hat{\gamma}_k), \quad (36a)$$

$$\text{subject to } (1 - \alpha_k) p_t \left| \sum_{i \in \mathcal{K}} \mathbf{f}_k^T \mathbf{w}_i \right|^2 \geq p'_b, \quad (36b)$$

$$0 < \alpha_k < 1. \quad (36c)$$

To solve \mathbf{P}_α , we first introduce θ_k to replace the SINR terms in (36a), such that $\theta_k \leq \hat{\gamma}_k$, and then reformulate \mathbf{P}_α as follows:

$$\mathbf{P}_{\alpha 1} : \underset{\alpha, \theta}{\text{maximize}} \sum_{k \in \mathcal{K}} \psi \log_2(1 + \theta_k), \quad (37a)$$

$$\text{subject to } \theta_k \leq \frac{\hat{A}_k(\alpha)}{\hat{B}_k(\alpha)}, \quad (37b)$$

$$(1 - \alpha_k) p_t |\mathbf{d}_k^T \mathbf{w}|^2 \geq p'_b, \quad (37c)$$

$$0 < \alpha_k < 1, \quad (37d)$$

where $\alpha = [\alpha_1, \dots, \alpha_K]^T$ and $\theta = [\theta_1, \dots, \theta_K]^T$. Besides, $\hat{A}_k(x)$ and $\hat{B}_k(x)$ are the numerators and denominators of the corresponding SINR terms $\hat{\gamma}_k$ as functions of the variable x i.e., α . The reformulated optimization problem $\mathbf{P}_{\alpha 1}$ can be considered as a two-part optimization problem, i.e., (i) an outer optimization over α with fixed θ and (ii) an inner optimization over θ with fixed α .

The inner optimization problem is thus given as

$$\mathbf{P}_{\alpha 2} : \underset{\alpha, \theta}{\text{maximize}} \sum_{k \in \mathcal{K}} \psi \log_2(1 + \theta_k), \quad (38a)$$

$$\text{subject to } \theta_k \leq \frac{\hat{A}_k(\alpha)}{\hat{B}_k(\alpha)}. \quad (38b)$$

This inner optimization problem in (38) is convex in θ and has strong duality [34]. Thus, the solution to $\mathbf{P}_{\alpha 2}$ is that θ_k satisfies (38b) with equality. We use the Lagrangian dual transform [34] to deal with the logarithm in the objective function of $\mathbf{P}_{\alpha 2}$, and the corresponding Lagrangian function is given as

$$L(\theta, \mu) = \sum_{k \in \mathcal{K}} \psi \log_2(1 + \theta_k) - \sum_{k \in \mathcal{K}} \mu_k \left(\theta_k - \frac{\hat{A}_k(\alpha)}{\hat{B}_k(\alpha)} \right), \quad (39)$$

where $\mu = [\mu_1, \dots, \mu_K]^T$ is the dual variable vector introduced for each inequality constraint in (38b). From the strong duality, $\mathbf{P}_{\alpha 2}$ is equivalently reformulated to a dual problem as follows:

$$\mathbf{P}_{\alpha 3} : \underset{\mu \geq 0}{\text{minimize}} \underset{\theta}{\text{maximize}} L(\theta, \mu). \quad (40)$$

The optimal solution of μ_k can then be obtained by evaluating the first-order condition $\partial L(\theta, \mu) / \partial \theta_k$ and applying the trivial solution to $\mathbf{P}_{\alpha 2}$ as

$$\mu_k^o = \frac{\psi \hat{B}_k(\alpha)}{\hat{A}_k(\alpha) + \hat{B}_k(\alpha)}. \quad (41)$$

Besides, $\mu_k \geq 0$ is automatically satisfied in this case. Using (39) and (41), $\mathbf{P}_{\alpha 2}$ is reformulated as

$$\mathbf{P}_{\alpha 4} : \text{maximize } L(\boldsymbol{\theta}, \boldsymbol{\mu}^o). \quad (42)$$

Further, it can be shown the solution to $\mathbf{P}_{\alpha 4}$ satisfies \mathbf{P}_{α} when combined with the outer optimization over $\boldsymbol{\alpha}$ and after several mathematical interpretations [34], [39]. Then, the tags' reflection coefficients, $\boldsymbol{\alpha}$, are obtained by solving feasibility problem over $\boldsymbol{\alpha}$ for fixed $\boldsymbol{\theta}$. The corresponding optimization problem is thus given as

$$\mathbf{P}_{\alpha 5} : \text{find } \boldsymbol{\alpha}, \quad (43a)$$

$$\text{subject to } \theta_k^o \leq \frac{\hat{A}_k(\boldsymbol{\alpha})}{\hat{B}_k(\boldsymbol{\alpha})}, \quad (43b)$$

$$(1 - \alpha_k)p_t |\mathbf{d}_k^T \mathbf{w}|^2 \geq p'_b, \quad (43c)$$

$$0 < \alpha_k < 1. \quad (43d)$$

Algorithm 2 provides the proposed approach for optimizing the tags' reflection coefficients.

Algorithm 2 : Reflection coefficient optimization.

Initialization: Initialize $\boldsymbol{\alpha}$ to a feasible value.

Repeat

Step 1: Update $\boldsymbol{\mu}$ by (41).

Step 2: Update $\boldsymbol{\theta}$ by solving $\mathbf{P}_{\alpha 4}$ in (42).

Step 3: Update $\boldsymbol{\alpha}$ by solving $\mathbf{P}_{\alpha 5}$ in (43).

Until the value of the objective function converges.

Output: The optimal reflection coefficients $\boldsymbol{\alpha}^o$.

Algorithm 3 : Overall algorithm.

Initialization: Initialize \mathbf{u}_k for $k \in \mathcal{K}$ and $\boldsymbol{\alpha}$ to a feasible values.

Repeat

Step 1: Update \mathbf{w} by solving \mathbf{P}_w in (25).

Step 2: Update \mathbf{u}_k for $k \in \mathcal{K}$ by solving \mathbf{P}_u in (33).

Step 3: Update $\boldsymbol{\alpha}$ by solving \mathbf{P}_{α} in (36).

Until the value of the objective function converges.

Output: The optimal beamforming \mathbf{w}^o , receiver combining \mathbf{u}_k^o , and reflection coefficients $\boldsymbol{\alpha}^o$.

Remark 6. Algorithm 3 presents the overall algorithm for solving the proposed optimization problem, $\mathbf{P1}$ (22). We begin by setting \mathbf{u}_k for $k \in \mathcal{K}$ and $\boldsymbol{\alpha}$ to feasible values. Then, in each iteration, algorithms update better solutions for \mathbf{w} , \mathbf{u}_k , and $\boldsymbol{\alpha}$ until the objective function no longer improves. The procedure is terminated when the normalized objective function increment is less than $\epsilon = 10^{-3}$.

D. Computational Complexity

The proposed AO solution is a multi-stage iterative algorithm. Here, the outer loop has three sub-problems for optimizing \mathbf{w} , \mathbf{u}_k for $k \in \mathcal{K}$, and $\boldsymbol{\alpha}$. Each sub-problem requires an iterative updating method to solve. Specifically, the computational complexity of Algorithm 1 lies in Step 2. Matlab CVX uses SDPT3 solver for solving the sub-problem for \mathbf{w} . Thus, the computational complexities of Algorithm Algorithm 1 is $\mathcal{O}(M^3 K^3)$ [40], [41]. The computational

complexity of the sub-problem for solving \mathbf{u}_k for $k \in \mathcal{K}$ is in the matrix inversion, multiplication, and eigenvalue decomposition (35). Hence, the computational complexity is $\mathcal{O}(K^3(2K^2+1))$. The computational complexity of Algorithm 2 lies in step 3. Similar to Algorithm 1, CVX Matlab uses an SDPT3 solver to handle this optimization problem. Therefore, the computational complexity of Algorithm 2 is $\mathcal{O}(M^3 K^3)$ [40], [41]. Hence, the total complexity of the proposed AO solution is $\mathcal{O}(I_o(I_w M^3 K^3 + K^3(2K^2 + 1) + I_{\alpha} M^3 K^3))$, where I_w , I_{α} , and I_o are the iteration numbers of Algorithm 1, Algorithm 2, and the overall algorithm (outer loop – Algorithm 3), respectively [40], [41].

E. Algorithm Convergence

As a well-established concept, the overall algorithm convergence in AO is guaranteed as long as the individual blocks within the AO algorithm converge [42].

In our proposed solution, we utilize the FP technique to solve \mathbf{w} and $\boldsymbol{\alpha}$ blocks, whereas \mathbf{u}_k for $k \in \mathcal{K}$ is obtained as a closed-form solution applying the Rayleigh ratio quotient approach. Hence, overall algorithm convergence relies on the FP. Interestingly, the FP yields a fixed-point iteration method with provable convergence [34], [41], [43], ensuring the convergence of our proposed AO method. Nonetheless, our simulation results also corroborate the validity of this claim (Fig. 5).

V. SIMULATION RESULTS

Herein, we present simulation examples for evaluating the performance of the proposed cell-free BiBC system.

We adopt a three-slope model for modeling the large-scale fading ζ_v (1) with operating frequency, f_c , in MHz [44]. In particular, for $d_0 = 10$ m and $d_1 = 50$ m, the path-loss exponent is (i) 3.5 if the distance between two nodes in m (denoted by d) is larger than d_1 , (ii) 2 if $d_1 \geq d > d_0$, and (iii) 0 if $d \leq d_0$. When $d > d_1$, the Hata-COST231 propagation model is employed. The path-loss in dB is then defined as

$$\zeta_v = \begin{cases} -L - 35 \log_{10}(d), & \text{if } d > d_1, \\ -L - 15 \log_{10}(d_1) - 20 \log_{10}(d), & \text{if } d_0 < d \leq d_1, \\ -L - 15 \log_{10}(d_1) - 20 \log_{10}(d_0), & \text{if } d \leq d_0, \end{cases} \quad (44)$$

where $L = 46.3 + 33.9 \log_{10}(f_c) - 13.82 \log_{10}(h_t) - (1.1 \log_{10}(f_c) - 0.7)h_r + (1.56 \log_{10}(f_c) - 0.8)$. Here, h_t and h_r denote the transmitter and receiver antenna heights in m, respectively, i.e., AP antenna height, h_{AP} , tag antenna height, h_T , and reader antenna height, h_R . The AWGN variance, σ^2 is modeled as $\sigma^2 = 10 \log_{10}(N_0 B N_f)$ dBm, where $N_0 = -174$ dBm/Hz, B is the bandwidth, and N_f is the noise figure.

To model the coverage area, e.g., warehouse, we consider a 100×100 m² square area, the reader is located at the center, the APs are uniformly distributed, and the tags are randomly distributed within the area. Unless otherwise specified, Table II gives the simulation parameters.

TABLE II: Simulation settings.

Parameter	Value	Parameter	Value
f_c	2 GHz	M	36
B	10 MHz	L	4
N_f	10 dB	K	{3, 5}
d_0, d_1	{10, 50}m	p_b	-20 dBm
h_{AP}, h_T, h_R	{15, 1, 1.6}m	p_p	20 dBm
τ_c	1000	τ_p	5

A. Channel Estimation

We first investigate the performance of our channel estimation method (section II-D), considering the LS estimator.

The quality of the channel estimator is assessed in terms of normalized MSE, which is defined as

$$\text{Normalized MSE} = \frac{\mathbb{E} \left\{ \|\mathbf{v} - \hat{\mathbf{v}}\|^2 \right\}}{\mathbb{E} \left\{ \|\mathbf{v}\|^2 \right\}}, \quad (45)$$

where $\mathbf{v} \in \{\mathbf{h}_{0,m}, \mathbf{h}_{k,m}, f_{k,m}\}$.

Fig. 4 shows the normalized MSE performance of the LS estimator versus the per-AP pilot transmit power p_p for the direct, cascaded, and forward channels, considering $K = 3$, and $\tau = \{5, 7, 11\}$. Our method demonstrates high accuracy in estimating all the channels for multiple tag scenarios. However, the cascaded and the forward channel normalized MSE have high values when compared to the direct channel normalized MSE. This is primarily due to the double path loss present in the cascaded and the forward channels and the tag's reflection coefficient α . We also observe that increasing the pilot sequence length improves the estimation accuracy and lowers the required transmit power for a given MSE level. For instance, for the direct link, a normalized MSE of 10^{-5} is achieved at 12 dBm and 16 dBm for $\tau = 11$ and $\tau = 5$, respectively. Similarly, increasing the pilot length from $\tau = 5$ and $\tau = 11$ can save 2.5 dBm dB and 2 dBm of transmit power, respectively, to obtain a normalized MSE of 2×10^{-2} in the forward channel and 5×10^{-3} in the cascaded channel.

Note that using the highly accurate estimates of the direct link channels, the reader is able to effectively cancel out the DLI, thereby justifying the assumption stated in Remark 2.

In the following, we use these channel estimates to evaluate the performance of our proposed schemes for the BiBC network, for $p_p = 20$ dBm, and $\tau = 5$.

B. Convergence Rate of the Proposed Algorithm

Before proceeding to the performance analysis, we investigate the convergence rate of the proposed algorithm (Section IV, Remark 6). To this end, Fig. 5 shows its convergence behavior for when the AP is at $p_t = \{0, 10, 20, 30\}$ dBm. The objective function of the overall algorithm is the sum rate. The stopping condition for convergence is that the increment of the normalized objective function is less than $\epsilon = 10^{-3}$. As shown in Fig. 5, the sum rate achieved by the overall Algorithm 3 increases rapidly and saturates as the number of iterations increases. Specifically, it converges in less than five iterations regardless of the AP transmit power.

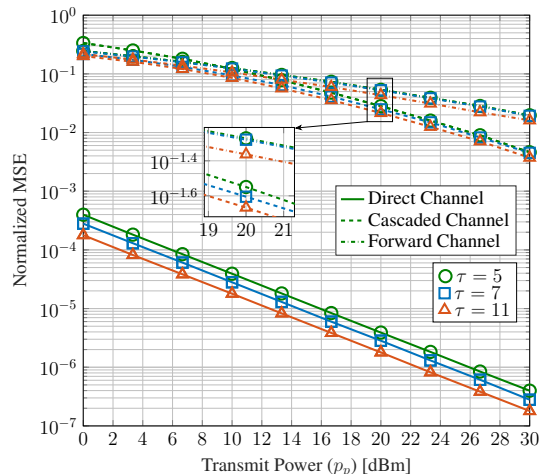


Fig. 4: Normalized MSE of direct, cascaded, and forward channels for $K = 3$, and $\tau = \{5, 7, 11\}$.

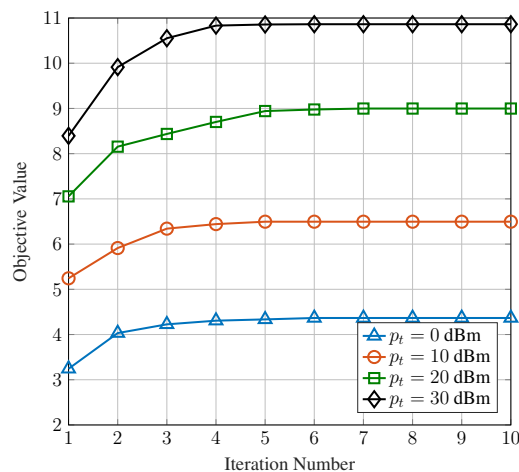


Fig. 5: The convergence of the objective value of the overall algorithm.

C. Performance Analysis

In this section, we assess the performance of the proposed cell-free BiBC network. We evaluate our power allocation and channel estimation schemes in terms their ability to enhance the received power at the tags and the sum rate. We consider two benchmarks alongside our proposed scheme:

A_1 *Random beamforming*: Optimal beamforming in a multi-antenna communication system relies on CSI. When CSI is unavailable, random beamforming may be used as an alternative, which might not seem ideal at first. To assess the effectiveness of random beamforming, we may compare it with optimal beamforming, assuming perfect CSI, in a system with M transmit antennas and n users. Surprisingly, in this scenario, both optimal and random beamforming achieve the same asymptotic sum-rate capacity of $M \log(n)$ [45], [46]. This observation justifies the use of random beamforming in cases where CSI is not available. To implement random beamforming, we choose complex Gaussian random vectors for \mathbf{w} and \mathbf{u}_k , ($k \in \mathcal{K}$), satisfying the per-AP transmit power con-

straint (22b) and the reader's normalized power constraint (22d), respectively. The advantage of this approach is that it requires no CSI. Additionally, the reflection coefficients are set to 0.6 in this specific case.

A_2 *Optimal beamforming with perfect CSI:* \mathbf{w} , \mathbf{u}_k ($k \in \mathcal{K}$), and α are obtained through the proposed optimization framework with perfect CSI, i.e., without performing channel estimation.

A_3 *Optimal beamforming with estimated CSI:* \mathbf{w} , \mathbf{u}_k ($k \in \mathcal{K}$), and α are obtained using the proposed optimization framework with estimated CSI using the proposed channel estimation.

1) *Received Power at the Tag:* Increasing this quantity is critical for ensuring that the tag can be activated.

To achieve this objective, we present in Fig. 6 and Fig. 7 the graphical representations of the received power experienced by a tag, delineated with respect to variations in transmit power and the number of APs. Notably, these figures also incorporate the activation threshold, $p_b = -20$ dBm, a reference point derived from established parameters for commercial RFID tags [7], thereby providing invaluable insights into our analysis. Examining Fig. 6 and Fig. 7 underscores the efficacy of our proposed channel estimation and optimization frameworks. Across a spectrum of transmit power settings and AP quantities, our frameworks consistently yield higher power delivery to the tags. In stark contrast, the utilization of random beamforming (A_1) necessitates escalated transmit power levels and an increased number of APs to attain the power threshold requisite for the tags. Illustratively, for instance, the A_1 approach mandates a minimum of 12 dBm when paired with 36 APs (Fig. 6), or 12 APs at 20 dBm (Fig. 7) to exceed the activation threshold. Evidently, from an energy efficiency perspective, random beamforming exhibits suboptimal performance. Our proposed algorithms clearly bring much-needed energy savings.

However, it is important to note that our proposed channel estimation scheme, while effective, falls short of the ideal performance achieved by perfect CSI benchmark A_2 . Despite this disparity, there are strategic measures to bridge the gap:

- 1) **Allocating higher transmit power at APs:** By boosting the power at APs, we can enhance the signal-to-noise ratio and mitigate the impact of imperfect channel estimation.
- 2) **Deploying more APs:** Increasing the density of APs can provide additional diversity and redundancy, which in turn can help compensate for the performance gap.
- 3) **Employing longer pilot sequences:** Longer pilot sequences offer finer granularity in channel estimation, allowing for improved accuracy even with non-ideal schemes.

In essence, while our proposed CSI estimation method may not attain perfection, it can harmoniously integrate with these complementary solutions to attain remarkably high-performance standards.

2) *Achievable Sum Rate:* The achievable sum rate of the tags is investigated in Fig. 8 and Fig. 9, for different numbers of tags $K = \{3, 5\}$.

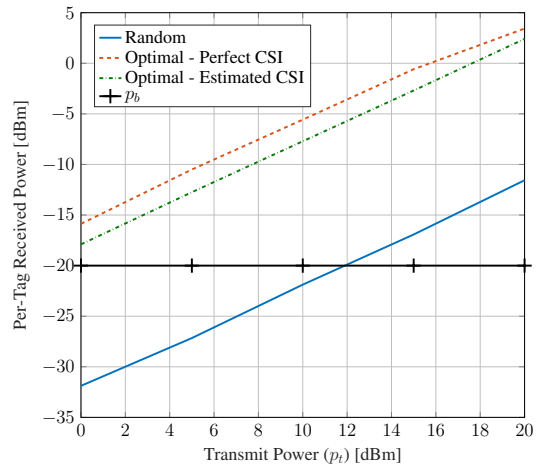


Fig. 6: Per-tag received power versus the transmit power.

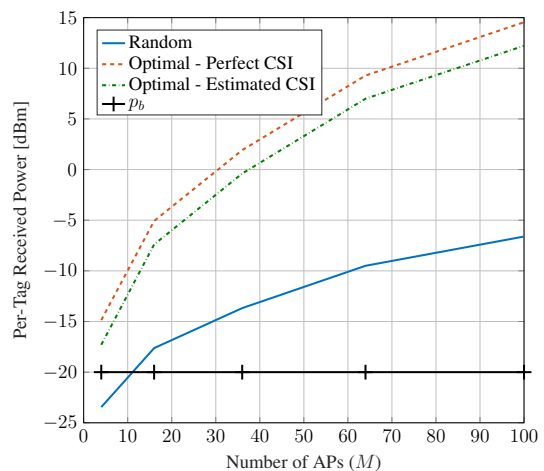


Fig. 7: Per-tag received power versus the number of APs for $p_t = 20$ dBm.

Fig. 8 illustrates the sum rate achieved by the tags as a function of the transmit power, p_t . It reveals that random beamforming designs, which do not rely on CSI, attain the lowest sum rate as they shape the beam in arbitrary directions. In contrast, our optimal beamforming designs achieve significant sum rates under both perfect and estimated CSI. Additionally, the achieved sum rate using the estimated CSI is comparable to that achieved with perfect CSI, demonstrating the efficiency of our channel estimation strategy. In particular, the optimal designs under perfect and estimated CSI improve the achieved sum rate respectively 425% and 375% compared to the random designs for $K = 5$, and $p_t = 10$ dBm.

Fig. 9 also depicts the achieved sum rate versus the number of APs for $p_t = 20$ dBm, and $K = \{3, 5\}$. As observed, unlike random designs, through optimal beamforming designs, the achieved sum rate significantly improves due to the efficient use of resources. These findings reveal the effectiveness of our proposed resource allocation and CSI estimation frameworks.

3) *Tags with Fixed and Reconfigurable α :* It is interesting to see how much performance gains are possible by going fixed

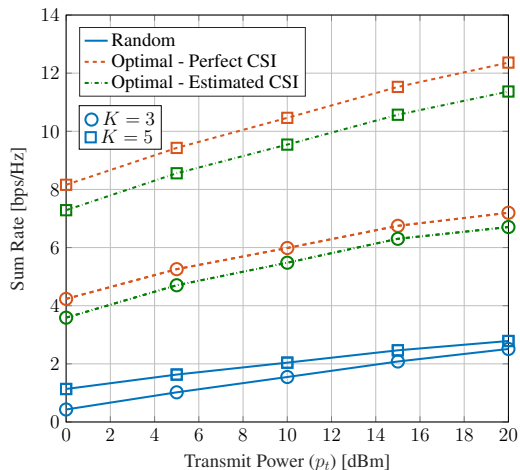


Fig. 8: Sum rate versus the transmit power.

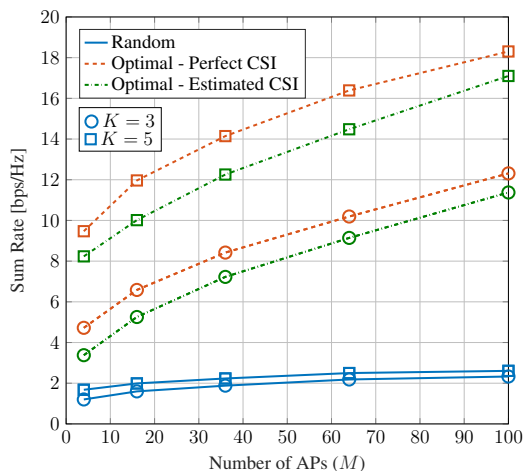


Fig. 9: Sum rate versus the number of APs for $p_t = 20$ dBm.

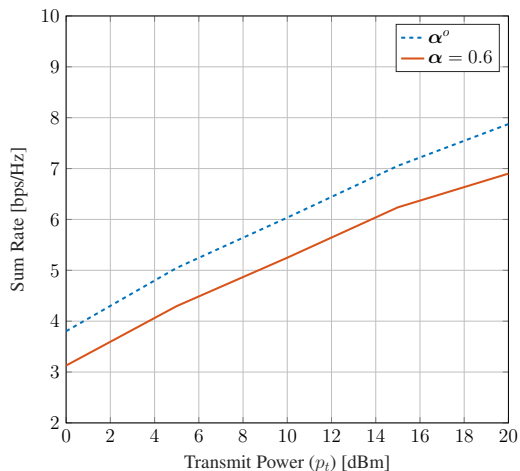


Fig. 10: Sum rate versus the transmit power for $K = 3$.

to variable tags. To this end, we compare the performances of tags with fixed and variable reflection coefficients. Thus, we evaluate fixed tags ($\alpha_k = 0.6$ for $k \in \mathcal{K}$) using the proposed

beamforming at APs and combining at the reader. We thus plot the achieved rates of the sum rate as a function of the AP transmit power in Fig. 10. As expected, when the tags use optimal α^o , the sum rate significantly improves. For example, the total sum rate achieves by the optimal α^o is ~ 1 bps/Hz at $p_t = 20$ dBm than that of the tags with fixed α . Furthermore, depending on the application requirements and environment, our optimization framework is flexible enough to handle either tags with fixed α or tags with variable α .

VI. CONCLUSION

We investigated the challenge of ensuring robust energy harvests for tags within a broad-ranging BiBC network, spanning extensive areas such as warehouses. Our proposed solution introduces a cell-free, distributed Access AP-assisted BiBC configuration, meticulously engineered to enhance EH reliability across multiple tags, thereby reducing their performance reliance on spatial positioning.

To achieve this objective, we introduced a channel estimation scheme tailored to accommodate the passive transmission characteristics of tags. Leveraging these channel estimates, we determined optimal beamforming weights at the APs, reflection coefficients at the tags, and combining vectors at the reader. Our aim was to maximize the aggregate tag data rate while satisfying the essential minimum energy requirements.

Notably, the optimization problems posed by these intricate scenarios are inherently non-convex. To address this challenge, we developed solution methods grounded in the Alternating Optimization, Fractional Programming, and Rayleigh Ratio Quotient approaches.

We emphasize that while our study was primarily developed with reconfigurable backscatter tags in mind, it is readily applicable to tags with fixed reflection coefficients. The latter option, characterized by its cost-effectiveness and simplicity, presents a viable networking alternative. Conversely, reconfigurable tags, while more costly, possess the potential to significantly enhance overall network performance.

In summary, our research lays the groundwork for the evolution of cell-free BiBC systems equipped to accommodate multiple tags, thus bolstering their readiness to support emerging IoT networks.

REFERENCES

- [1] "3GPP TSG RAN -94e, Moderator's summary for discussion [RAN94e-R18Prep-28] passive IoT (from RP-212688)," Dec. 2021. Available Online: <https://portal.3gpp.org/ngppapp/TdocList.aspx?meetingId=60043>.
- [2] "3GPP TSG RAN -97e3, Study on ambient IoT , 9.1 (from RP-222685)," Sept. 2022. Available Online: <https://portal.3gpp.org/ngppapp/TdocList.aspx?meetingId=60043>.
- [3] "3GPP TSG RAN Meeting -94e, Study proposal on passive IoT, 8A.1 (from RP-213368)," Dec. 2021. Available Online: <https://www.3gpp.org/DynaReport/TDocExMtg--RP-94-e--60214.htm>.
- [4] D. Galappaththige, F. Rezaei, C. Tellambura, and S. Herath, "Link budget analysis for backscatter-based passive IoT," *IEEE Access*, vol. 10, pp. 128890–128922, Dec. 2022.
- [5] F. Rezaei, D. Galappaththige, C. Tellambura, and S. Herath, "Coding techniques for backscatter communications - a contemporary survey," *IEEE Commun. Surveys Tuts.*, pp. 1–1, 2th Quat. 2023.
- [6] D. T. Hoang, D. Niyato, D. I. Kim, N. V. Huynh, and S. Gong, *Ambient Backscatter Communication Networks*. Cambridge University Press, 2020.

- [7] “GAO RFID Inc.,” Available Online: <https://gaorfid.com/>.
- [8] H. Q. Ngo, L. Tran, T. Q. Duong, M. Matthaiou, and E. G. Larsson, “On the total energy efficiency of cell-free massive MIMO,” *IEEE Trans. Green Commun. Netw.*, vol. 2, pp. 25–39, Mar. 2018.
- [9] E. Nayeibi, A. Ashikhmin, T. L. Marzetta, H. Yang, and B. D. Rao, “Pre-coding and power optimization in cell-free massive MIMO systems,” *IEEE Trans. Wireless Commun.*, vol. 16, pp. 4445–4459, Jul. 2017.
- [10] D. Galappaththige and G. Amarasureiya, “Cell-free massive MIMO with underlay spectrum-sharing,” in *IEEE Int. Conf. Commun. (ICC)*, pp. 1–7, May 2019.
- [11] Z. Dai, R. Li, J. Xu, Y. Zeng, and S. Jin, “Rate-region characterization and channel estimation for cell-free symbiotic radio communications,” *IEEE Trans. Commun.*, vol. 71, pp. 674–687, Feb. 2023.
- [12] X. Jia and X. Zhou, “Power beacon placement for maximizing guaranteed coverage in bistatic backscatter networks,” *IEEE Trans. Commun.*, vol. 69, pp. 7895–7909, Nov. 2021.
- [13] Z. Dai, R. Li, J. Xu, Y. Zeng, and S. Jin, “Cell-free symbiotic radio: Channel estimation method and achievable rate analysis,” in *IEEE/CIC Int. Conf. Commun. in China (ICCC Workshops)*, pp. 25–30, Jul. 2021.
- [14] K. Han and K. Huang, “Wirelessly powered backscatter communication networks: Modeling, coverage, and capacity,” *IEEE Trans. Wireless Commun.*, vol. 16, pp. 2548–2561, Apr. 2017.
- [15] F. Rezaei, D. Galappaththige, C. Tellambura, and A. Maaref, “Time-spread pilot-based channel estimation for backscatter networks,” *arXiv preprint arXiv:2305.17248*, 2023.
- [16] M. Hua, L. Yang, C. Li, Z. Zhu, and I. Lee, “Bistatic backscatter communication: Shunt network design,” *IEEE Internet Things J.*, vol. 8, pp. 7691–7705, May 2021.
- [17] A. Kaplan, J. Vieira, and E. G. Larsson, “Dynamic range improvement in bistatic backscatter communication using distributed MIMO,” in *IEEE Global Commun. Conf.*, pp. 2486–2492, Dec. 2022.
- [18] Q. Tao, Y. Li, C. Zhong, S. Shao, and Z. Zhang, “A novel interference cancellation scheme for bistatic backscatter communication systems,” *IEEE Commun. Lett.*, vol. 25, pp. 2014–2018, Jun. 2021.
- [19] G. Sacarello, M. Awais, and Y. H. Kim, “Bistatic backscatter NOMA with transmit and receive beamforming,” in *Int. Conf. Inf. Commun. Techn. Converg. (ICTC)*, pp. 851–853, Oct. 2021.
- [20] H. Yang, Y. Ye, K. Liang, and X. Chu, “Power beacon energy consumption minimization in wireless powered backscatter communication networks,” *Early Access*, Apr. 2023.
- [21] H. Yang, Y. Ye, and X. Chu, “Max-min energy-efficient resource allocation for wireless powered backscatter networks,” *IEEE Wireless Communications Letters*, vol. 9, pp. 688–692, May 2020.
- [22] L. Qu, D. Mishra, and J. Yuan, “Channel estimation protocol for bistatic backscattering using multi-antenna transceiver,” in *IEEE 33rd Annual Int. Symposium on Personal, Indoor and Mobile Radio Commun. (PIMRC)*, pp. 439–444, Sept. 2022.
- [23] M. Yezhanova and Y. H. Kim, “Channel estimation via model and learning for monostatic multi-antenna backscatter communication,” *IEEE Access*, vol. 9, pp. 165341–165350, Dec. 2021.
- [24] Y. Liao, G. Yang, and Y.-C. Liang, “Resource allocation in NOMA-enhanced full-duplex symbiotic radio networks,” *IEEE Access*, vol. 8, pp. 22709–22720, Jan. 2020.
- [25] G. Yang, D. Yuan, Y.-C. Liang, R. Zhang, and V. C. M. Leung, “Optimal resource allocation in full-duplex ambient backscatter communication networks for wireless-powered IoT,” *IEEE Internet Things J.*, vol. 6, pp. 2612–2625, Apr. 2019.
- [26] Ö. Demir, E. Björnson, and L. Sanguinetti, *Foundations of User-Centric Cell-Free Massive MIMO*. Foundations and trends in signal processing, Now Publishers, 2021.
- [27] D. Galappaththige, F. Rezaei, C. Tellambura, and S. Herath, “RIS-empowered ambient backscatter communication systems,” *IEEE Wireless Commun. Lett.*, vol. 12, pp. 173–177, Jan. 2023.
- [28] D. Wang, F. Rezaei, and C. Tellambura, “Performance analysis and resource allocations for a WPCN with a new nonlinear energy harvester model,” *IEEE open j. Commun. Soc.*, vol. 1, pp. 1403–1424, Sept. 2020.
- [29] D. Galappaththige and G. Aruma Baduge, “Exploiting distributed IRSs for enabling SWIPT,” *IEEE Wireless Commun. Lett.*, vol. 11, pp. 673–677, Apr. 2022.
- [30] R. Long, Y.-C. Liang, H. Guo, G. Yang, and R. Zhang, “Symbiotic radio: A new communication paradigm for passive internet of things,” *IEEE Internet Things J.*, vol. 7, pp. 1350–1363, Feb. 2020.
- [31] D. Tse and P. Viswanath, *Fundamentals of Wireless Communication*. Cambridge University Press, 2005.
- [32] Q. Zhang, S. Jin, K.-K. Wong, H. Zhu, and M. Matthaiou, “Power scaling of uplink massive MIMO systems with arbitrary-rank channel means,” *IEEE J. Sel. Topics Signal Process.*, vol. 8, pp. 966–981, Oct. 2014.
- [33] S. Stanczak, M. Wiczanowski, and H. Boche, *Fundamentals of Resource Allocation in Wireless Networks: Theory and Algorithms*. Springer Publishing Company, Incorporated, 2nd ed., 2009.
- [34] K. Shen and W. Yu, “Fractional programming for communication systems—part I: Power control and beamforming,” *IEEE Trans. Signal Process.*, vol. 66, pp. 2616–2630, May 2018.
- [35] D. Galappaththige, D. Kudathanthirige, G. Amarasureiya, and C. Tellambura, “Weighted sum-rate maximization for distributed RIS-assisted cell-free massive MIMO,” in *IEEE Conf. Standards for Commun. Netw. (CSCN)*, pp. 236–241, Nov. 2022.
- [36] S. Boyd and L. Vandenberghe, *Convex Optimization*. Cambridge University Press, Mar. 2004.
- [37] S. Stanczak, *Fundamentals of Resource Allocation in Wireless Networks Theory and Algorithms*. Berlin, Heidelberg: Springer Berlin Heidelberg, 2nd ed., 2008.
- [38] W. Wan, X. Wang, J. Yang, and B. Zhao, “Joint linear pre-coder and combiner optimization for distributed antenna systems,” in *IEEE Global Commun. Conf. (GLOBECOM)*, pp. 1–6, Dec. 2016.
- [39] H. Guo, Y.-C. Liang, J. Chen, and E. G. Larsson, “Weighted sum-rate maximization for intelligent reflecting surface enhanced wireless networks,” in *Global Commun. Conf. (GLOBECOM)*, pp. 1–6, Dec. 2019.
- [40] A. Ben-Tal and A. S. Nemirovskii, *Lectures on Modern Convex Optimization: Analysis, Algorithms, and Engineering Applications*. USA: Society for Industrial and Applied Mathematics, 2001.
- [41] J. S. Borrero, C. Gillen, and O. A. Prokopyev, “Fractional 0–1 programming: Applications and algorithms,” *J. of Global Optimization*, vol. 69, pp. 255–282, Sept. 2017.
- [42] J. C. Bezdek and R. J. Hathaway, “Convergence of alternating optimization,” vol. 11, Dec. 2003.
- [43] K. Shen, *Fractional Programming for Communication System Design*. Phd thesis, University of Toronto, Ontario, Canada, June 2020. Available at <https://tspace.library.utoronto.ca/handle/1807/101285>.
- [44] H. Q. Ngo, A. Ashikhmin, H. Yang, E. G. Larsson, and T. L. Marzetta, “Cell-free massive MIMO versus small cells,” *IEEE Trans. Wireless Commun.*, vol. 16, pp. 1834–1850, Mar. 2017.
- [45] J. Chung, C.-S. Hwang, K. Kim, and Y. K. Kim, “A random beamforming technique in MIMO systems exploiting multiuser diversity,” *IEEE J. Sel. Areas Commun.*, vol. 21, pp. 848–855, Jun. 2003.
- [46] M. Sharif and B. Hassibi, “On the capacity of MIMO broadcast channel with partial side information,” in *Proc. 37 Asilomar Conf. Signals, Systems & Computers*, vol. 1, pp. 958–962, Nov. 2003.